Modifications in Retinal Mitochondrial Respiration Precede Type 2 Diabetes and Protracted Microvascular Retinopathy

Woo Hyun Han,[1] Jonathan Gotzmann,[2] Sharee Kuny,[1] Hui Huang,[2] Catherine B. Chan,[2,3] Hélène Lemieux,[4] and Yves Sauvé[1,2]

[1]Department of Ophthalmology and Visual Sciences, University of Alberta, Edmonton, Alberta, Canada
[2]Department of Physiology, University of Alberta, Edmonton, Alberta, Canada
[3]Agriculture, Food and Nutritional Science, University of Alberta, Edmonton, Alberta, Canada
[4]Faculty Saint-Jean, University of Alberta, Edmonton, Alberta, Canada

Correspondence: Yves Sauvé, Department of Physiology, 7-55 Medical Sciences Building, University of Alberta, Edmonton, AB T6G 2H7, Canada;
ysauve@ualberta.ca.

WHH and JG are joint first authors.

Submitted: March 24, 2017
Accepted: June 28, 2017

Citation: Han WH, Gotzmann J, Kuny S, et al. Modifications in retinal mitochondrial respiration precede type 2 diabetes and protracted microvascular retinopathy. *Invest Ophthalmol Vis Sci*. 2017;58:3826–3839. DOI: 10.1167/iovs.17-21929

Purpose. To characterize retinal mitochondrial respiration associated with type 2 diabetes (T2D) progression in a cone-rich diurnal rodent, the Nile rat (genus *Arvicanthis*, species *niloticus*).

Methods. Nile rats were fed a standard rodent diet that resulted in rising glucose levels from 6 months. Age-matched control animals were fed a high-fiber diet that prevented diabetes up to 18 months. The functional status of specific retinal mitochondrial components and mitochondrial outer membrane integrity were studied by using high-resolution respirometry. Ocular complications were documented with funduscopy, electroretinography (ERG), and trypsin digestion of retinal vasculature.

Results. Mitochondrial functional changes were detected during hyperinsulinemia with maintained normoglycemia (2 months), corresponding to stage 1 of human T2D. Our data showed increased contribution of mitochondrial respiration through the NADH pathway relative to maximal oxidative phosphorylation capacity, with simultaneous electron entry into NADH (Complex I and related dehydrogenases) and succinate (Complex II) pathways. These compensatory events coincided with compromised mitochondrial outer membrane integrity. The first clinical sign of retinopathy (pericyte loss) was only detected at 12 months (after 6 months of sustained hyperglycemia) alongside a common ocular complication of diabetes, cataractogenesis. Further prolongation of hyperglycemia (from 12 to 18 months) led to capillary degeneration and delayed photopic ERG oscillatory potentials.

Conclusions. Oxidative phosphorylation compensatory changes in the retina can be detected as early as 2 months, before development of hyperglycemia, and are associated with reduced mitochondrial outer membrane integrity.

Keywords: hyperinsulinemia, hyperglycemia, type 2 diabetes, animal model, oxidative phosphorylation

With a worldwide prevalence of 415 million and importantly, estimates that only one of every two adults has been diagnosed,[1] the number of individuals living with diabetes may be closer to 1 billion. In adults, type 2 diabetes (T2D) accounts for most (90%–95%) diagnosed cases of diabetes.[2] A well-recognized microvascular complication of diabetes is diabetic retinopathy (DR).

Clinically, DR is an inner retina pathology that begins with the nonproliferative form characterized by alterations in blood flow, death of retinal pericytes, and basement membrane thickening.[3,4] Subsequently, the disease progresses to nonperfusion, microaneurysms, vascular loops, and hemorrhages evident on ophthalmic examination.[5] Ultimately, DR evolves to a proliferative stage, typified by neovascularization, neurodegeneration, and retinal detachment, which cause irreversible vision loss.[6] The cellular mechanisms underlying microvascular complications involve neurovascular cross talk, which is currently under intense scrutiny.[7] There is accumulating evidence that the outer retina, although asymptomatic itself, contributes to these microvascular changes.[8,9] Photoreceptor inner segments, in view of their extremely high metabolic activity,[10] their constitutive production of high amounts of reactive oxygen species (ROS),[11] and their high capacity for mitochondrial oxidative phosphorylation,[12] are attracting increasing attention in the pathophysiology of DR.[13]A major hurdle in identifying early pathologic events in DR has been the prevalence of animal models with early onset of diabetes.[13–15] In this study, we relied on the combined advantages of the laboratory rodent *Arvicanthis niloticus*: (1) it is a well-established model of T2D[16–18] and of associated retinopathy[19]; (2) unlike mouse and rat models, retinopathy progresses in a cone-rich retina (30%–35%, as opposed to 1%–2% in mouse and rat),[20,21] therefore more closely approximating the human macula (cone-dominated area); and (3) unlike mice and rats, Nile rats are diurnal, as humans are.[22] The latter advantage is particularly pertinent in the context that development of T2D

has been associated with circadian rhythm disruption via the dysregulation of clock genes.[23]

During development of T2D, Nile rats undergo an initial compensation for insulin resistance with increased insulin secretion at 2 months, followed by rising glucose levels from 6 months, increasing β-cell dysfunction and associated endoplasmic reticulum stress at 12 months, and finally, severe decompensation and progression to ketosis at 18 months.[16–18] Of note, feeding of a high-fiber diet completely prevents T2D in Nile rats.[18] Noda et al.[19] have described the protracted accumulation of leukocytes in retinal arteries at high plasma insulin levels, which is correlated with plasma leptin (body fat) in this model, and furthermore, demonstrated microvascular biomarkers of human early DR,[24] including tortuosity, acellular capillaries, and pericyte ghosts, all of which corroborate pericyte apoptosis. Hajmousa et al.[25] have attributed pericyte apoptosis, in vitro, to hyperglycemia-induced accumulation of ROS. Long-term exposure of "pericyte-like" adipose-derived stromal cells to hyperglycemia is also associated with impaired glucose uptake and mitochondrial electron transport system capacity measured in the intact cells after uncoupling.[25]

While mitochondrial dysfunction has been extensively studied in T2D, with distinct links between obesity, inactivity, and energy homeostasis, a causal relationship has yet to be established for the development of DR.[26] Deficiencies in mitochondrial biogenesis and/or activity, as well as chronic imbalances in energy metabolism, have been documented[27–29] in tissues other than the retina (such as muscle, liver, and pancreas), with healthy aging and across all T2D stages: (1) insulin sensitive with normal oxidative capacity and load; (2) prediabetic with compensation for insulin resistance characterized by low oxidative capacity (inactivity, aging), increased oxidative load (overnutrition, obesity) and associated with initially increased mitochondrial biogenesis; but incomplete oxidation ultimately leads to accumulation of lipid intermediates, fatty acid oxidation products, and ROS that induce (3) compensation failure and insulin secretory dysfunction (hyperglycemia). In the retina, alterations in mitochondrial membrane structure have been documented in hyperglycemia-induced DR.[30] Using the streptozotocin-injected (STZ) rat model of type 1 diabetes, Zhong and Kowluru[30] report enlarged mitochondria with loss of cristae in retinal microvasculature, which persist after reversal to normoglycemia.

Here, we took advantage of the long-term beta-cell compensation and T2D prevention in control Nile rats fed high-fiber diet versus those fed standard diet, in which compensation fails, to examine the interplay in the retina between early dysregulation of glucose metabolism and mitochondrial oxidative phosphorylation changes in a prediabetic stage before clinical manifestation of DR.

Methods

Animals and Diets

This study was performed on male Nile rats (*Arvicanthis niloticus*) aged 2 to 18 months; females were excluded on the basis of their reduced susceptibility to develop T2D[17] and to control for potential sexual dimorphisms with respect to metabolic pathways. After weaning at 21 days, animals were divided into two diet groups: (1) prediabetic and diabetic animals fed standard rodent diet (9.6% fat, 3.2% fiber, Prolab RMH 2000, 5P06; LabDiet, Nutrition Intl., Richmond, IN, USA), known to induce hyperinsulinemia by 2 months, followed by hyperglycemia from 6 months and decompensation at 18 months[18]; or (2) control animals fed high-fiber diet (4.1% fat, 15.0% fiber, Mazuri Chinchilla Diet, 5M01; Purina Mills, LLC, St. Louis, MO, USA), normoglycemic to 18 months. Food and water were provided ad libitum. Animals were maintained on a 14:10 light–dark cycle, room temperature 21°C ± 2°C, and relative humidity ~40%. This research was done under the approval of the Institutional Animal Care and Use Committee (University of Alberta). Experiments were carried out in accordance with National Institutes of Health (Bethesda, MD, USA) guidelines regarding the care and use of animals for experimental procedures and the ARVO Statement for the Use of Animals in Ophthalmic and Visual Research.

Fasting Blood Glucose, Glycated Hemoglobin, and Plasma Insulin

Fasting blood glucose (FBG) values were measured from tail blood samples after overnight (16–18 hours) fasting by using an Accu-chek Compact Plus glucose monitoring system (Roche, Mississauga, ON, Canada). Hyperglycemia was determined as FBG levels > 5.6 mM (100 mg/dL) as previously described.[18]

Nile rats were euthanized with a lethal dose (480 mg/kg) of Euthanyl (Bimeda-MTC Animal Health, Inc., Cambridge, ON, Canada). When animals reached surgical plane, cardiac puncture was performed and blood was collected in K_2EDTA-coated BD Microtainer Tubes with Microgar Closures (Becton, Dickinson and Company, Mississauga, ON, Canada). After centrifugation at 1000*g* for 20 minutes at 4°C, plasma was collected and stored at –80°C until use.

Plasma insulin levels were assessed by using an insulin ELISA kit (Ultra Sensitive Mouse Insulin ELISA kit No. 90080; Crystal Chem, Inc., Downers Grove, IL, USA). Fasting insulin levels > 2 ng/mL were indicative of compensation as previously described.[18]

Glycated hemoglobin (HbA1c) was measured by using a GLYCO-Tek affinity column kit (No. 5351; Helena Laboratories, Beaumont, TX, USA). Absorbance was measured at 415 nm. Percentage of HbA1c in the sample was calculated as recommended by the manufacturer. Nile rats with HbA1c levels > 6.5% were considered diabetic, as previously defined.[18,31]

Funduscopy

Nile rats were anaesthetized by using ketamine:xylazine (75:30 mg/kg). Eyes were dilated with corneal application of 1% tropicamide and 2.5% phenylephrine and kept hydrated with Tear-gel (Novartis Pharmaceuticals Canada, Inc., Mississauga, ON, Canada). Images from both eyes were captured with a Micron III retina imaging system for rodents (Phoenix Research Laboratories, Inc., Pleasanton, CA, USA) equipped with a Semrock FF01-554/211 filter for white light, FF01-469/35 exciter, and BLP01-488R barrier filters for blue excitation with green emission (Semrock, Inc., Rochester, NY, USA) and StreamPix 5 software (NorPix, Montreal, QC, Canada). Fluorescein angiography images were captured after intraperitoneal injection with fluorescein (1.5 μL/g body weight of 100 mg/mL fluorescein in PBS, F6377; Sigma, Oakville, ON, Canada).

Trypsin Digestion of Retinal Vasculature

After overnight fixation (16–18 hours) in 4% paraformaldehyde, retinas were removed and immersed in 3% trypsin in 0.1 M Tris, pH 7.8 (preheated to 37°C) for 130 minutes. Following digestion, the vitreous was carefully removed and the retina was subjected to gentle trituration with water to separate disintegrated neuronal tissue from the vasculature. Isolated vascular networks were mounted, treated with periodic acid

solution, and stained with Schiff's reagent and hematoxylin (Periodic Acid–Schiff kit 395B-1KT; Sigma-Aldrich Corp., St. Louis, MO, USA).

Pericytes were identified as round, dark extracapillary protrusions when compared to endothelial cells, which were oval and lighter in color.[32] Images were captured on a Reichert Polyvar 2 microscope with Infinity Analyze imaging software (Lumenera Corporation, Ottawa, ON, Canada) using an ×40 oil objective. Counts of pericytes, endothelial cells, and degenerated capillaries were performed and normalized to capillary area by using ImageJ 1.48v software (http://imagej.nih.gov/ij; provided in the public domain by the National Institutes of Health, Bethesda, MD, USA). Pericytes were categorized into three subtypes by location; pericytes located on straight capillaries, forked capillaries, and bridged between capillaries were classified as longitudinal, forked, and bridging pericytes, respectively. Six diabetic and six control animals were assessed at each time point (6, 12, and 18 months), and five randomly selected images per animal were analyzed. All variables met the criteria of normality and homogeneity of variance for ANOVA as tested with Kolmogorov-Smirnov (Lilliefors' correction) and Spearman tests, respectively. Therefore, differences between diet groups could be analyzed by using 2-way ANOVA with Bonferroni post hoc comparisons. Significance was set to $P < 0.05$.

Immunohistochemistry

After enucleation, corneas were punctured, and eyes were fixed in 4% paraformaldehyde for 30 minutes at 4°C. Corneas and lenses were carefully removed, and posterior eyecups were fixed a further 30 minutes, cryoprotected in sucrose (10% and 20% for 1 hour each, 30% overnight), embedded in O.C.T. (Tissue-Tek; Sakura Finetek, Torrance, CA, USA), frozen in liquid nitrogen, and stored at –80°C.

For cross sections, 20-µm cryosections were cut along the nasotemporal axis. After blocking in 10% normal serum and 0.3% Triton X-100 in PBS for 2 hours, sections were reacted overnight with goat anti–choline acetyl transferase (ChAT, 1:200, AB144P; Chemicon, Etobicoke, ON, Canada). All incubations were performed at room temperature. The following day sections were washed (3 × 5 minutes) in PBS and reacted for 2 hours with donkey anti-goat Alexa594 antibody (1:500; Molecular Probes, Inc., Eugene, OR, USA). After washing in PBS, slides were coated with ProLong Gold antifade reagent with DAPI (Life Technologies, Carlsbad, CA, USA) and coverslipped. Images were captured from the central and peripheral retina on a Leica DM6000B fluorescence microscope with DFC360FX camera and LAS AF v2.2.0 software (Leica Microsystems, Inc., Concord, Ontario, Canada), using a HC PL FLUORTAR 20.0x0.50 DRY objective (448.60-µm window). Brightness and contrast were adjusted by using Adobe Photoshop CC 2015 software (Adobe Systems, San Jose, CA, USA).

ChAT-immunoreactive amacrine cells and displaced amacrine cells (found in the ganglion cell layer [GCL]) were counted on both sides of the optic nerve and averaged (±standard deviation). Outer nuclear layer (ONL) and inner nuclear layer (INL) thickness measures were performed in the same manner. Comparisons were made by using Mann-Whitney U test. Significance was set to $P < 0.05$.

For whole retina flatmounts, retinas were washed extensively (6 × 30 minutes) in PBS + 0.1% tween-20 + 0.3% Triton X-100 and then blocked for 2 hours in 5% normal goat (or horse) serum in same, with shaking at room temperature for both steps. Flatmounts were then reacted with either goat anti–4-hydroxynonenal (4-HNE, 1:200, ab46544; Abcam, Cambridge, UK) or mouse anti-nitrotyrosine (1:100, 189542; Cayman Chemical, Ann Arbor, MI, USA) diluted in PBS + 0.3% Triton X-100 for 4 days at 4°C. After washing as before, flatmounts were incubated with species-appropriate Alexa488 secondary antibodies (1:1000) + DyLight 594 *Lycopersicon esculentum* (tomato) Lectin (1:100, DL-1177; Vector Laboratories, Burlingame, CA, USA) in a 1:10 dilution of blocking solution for 2 days at 4°C. After final washing, retinas were mounted ganglion cell side up in Fluoromount Aqueous Mounting Media (F4680-25ML; Sigma-Aldrich Corp.) and coverslipped. Images were captured as above.

ERG Recordings

ERGs were recorded at 18 months ($n = 6$ diabetic animals, $n = 3$ control animals). Nile rats were dark-adapted 1 hour before recording, and all subsequent preparations were made under dim red light. Animals were anesthetized with inhaled isofluorane (Somnosuite, Small Animal Anesthesia System; Kent Scientific, Torrington, CT, USA) and placed over a homeothermic blanket to maintain their body temperature at 38°C. Pupils were dilated with one drop of 1% tropicamide, and corneas were kept hydrated with methylcellulose. ERG recordings were performed as previously described.[20] Data were analyzed in a single eye per animal, selected on the basis of largest maximal a-wave amplitude in the scotopic intensity series. For oscillatory potential (OP) analysis, to ensure consistency between traces, amplitudes and implicit times were calculated by manually placing cursors at the base and apex of the first four OPs; cursors were sequentially labeled from 1 to 8 and values (amplitude or implicit time) were plotted for each cursor against stimulus strength.

Scotopic ERG. Intensity response series in dark-adapted animals were generated by presenting flashes (10-µs duration, 6500°K, xenon bulb) ranging between –3.70 to 2.86 log cd s/m^2 in luminance over 16 consecutive incremental steps. Intensity levels were measured with a photometer at the cornea level. Interstimulus intervals ranging from 10 seconds to 2 minutes were used for lowest to highest intensity flashes, respectively, providing sufficient time for rods to recover from photobleaching. Responses were recorded three to six times and averaged to optimize signal-to-noise ratio. For all recordings, a-wave amplitude corresponded to the difference between baseline at time 0 second (flash delivery) and negative a-wave trough, while b-wave amplitude corresponded to the difference between negative a-wave trough and positive b-wave peak (excluding OPs). Criterion amplitudes were set to 10 µV.

Mesopic ERG. After completion of scotopic ERG recordings, animals were exposed to a background illumination of 0.01 cd/m^2 for 10 minutes before applying the same tests as described above.

Photopic ERG. Finally, after completion of mesopic ERG recordings, animals were light-adapted at 30 cd/m^2 background for 10 minutes. Intensity response series were generated by presenting white flashes ranging between –1.63 to 2.86 log cd s/m^2 in luminance over 11 consecutive incremental steps. Responses were recorded six times and averaged. Interstimulus intervals of 3 seconds were used. Flicker response series were then recorded to flashes of 1.36 log cd s/m^2 presented at the following 13 incremental frequencies: 3, 5, 10, 15, 20, 25, 30, 35, 40, 45, 50, 55, and 60 Hz. The first 3 seconds were not harvested, avoiding averaging responses to single flashes. Amplitudes were measured from adjacent trough to peak and latencies from flash onset to peak.

Statistical comparison for each marker (1 to 8) was assessed with nonparametric Kruskal-Wallis 1-way analysis of variance. Significance was set to $P < 0.05$.

Investigative Ophthalmology & Visual Science

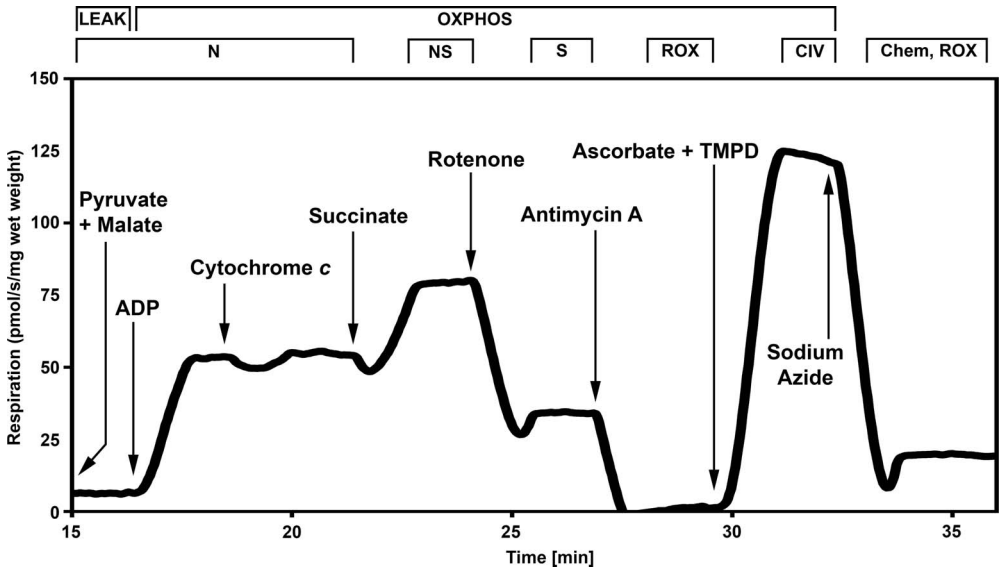

FIGURE 1. Representative trace of high-resolution respirometry using a multiple substrate-inhibitor-titration protocol in retinas from a single Nile rat. The oxygen consumption (*y*-axis) is represented as a function of time (*x*-axis). *Arrows* indicate times of titrations of substrates and inhibitors. The protocol includes the following steps: pyruvate+malate (added before the homogenate, N, NADH pathway, -LEAK state), ADP (N pathway, OXPHOS capacity); cytochrome *c* (integrity of outer mitochondrial membrane; damaged membrane allows exogenous cytochrome *c* to enter the intermembrane space, causing an increase in respiration), succinate (NADH and succinate pathway, NS, OXPHOS capacity), rotenone (inhibition of Complex I, S, succinate pathway, S, OXPHOS capacity), antimycin A (inhibition of Complex III, ROX), ascorbate+TMPD (CIV, Complex IV- OXPHOS capacity), sodium azide (inhibition of Complex IV, chemical background, Chem, ROX).

High-Resolution Respirometry

High-resolution respirometry (Oxygraph 2k; OROBOROS Instruments, Innsbruck, Austria) was performed by using freshly isolated retinas from individual Nile rats from 2 to 18 months (n = 5–12 per group, replicate measurements from a single animal were pooled). The oxygraph was calibrated at 37°C as per manufacturer's instructions with each chamber filled with 2 mL Mitochondrial Respiration Medium 05 (MiR05; 0.5 mM EGTA, 3 mM $MgCl_2 \cdot 6H_2O$, 60 mM K-lactobionate, 20 mM taurine, 10 mM KH_2PO_4, 20 mM HEPES, 110 mM sucrose, and 1 g/L BSA essentially fatty-acid free, pH 7.1).[33] Datlab software (OROBOROS Instruments) was used for data acquisition and analysis.

Wet weight was measured and retinas were immediately transferred into 1 mL ice-cold MiR05. Retinas were homogenized on ice with a Potter-Elvehjem attached to an overhead stirrer (Wheaton Instruments, Millville, NJ, USA). After five passes at intensity level two, 200 µL homogenate was immediately placed in each oxygraph chamber containing 1.8 mL MiR05. The remaining homogenate was frozen at −80 °C for determination of total protein (Pierce BCA protein assay kit, Cat. No. PI-23227; Thermo Fisher Scientific, Rockford, IL, USA) and citrate synthase (CS) activity (according to Kuznetsov et al.[34]). CS (EC 4.1.3.7) was measured at 37 °C with a UV/Vis spectrophotometer (Ultrospec 2100 Pro; Biochrom, Cambridge, MA, USA) equipped with a thermostated cell holder and a circulating water bath. After thawing the sample on ice, an additional cycle of homogenization with a conical glass homogenizer for 30 seconds on ice was performed to ensure complete homogeneity of the sample. The absorbance was measured at 412 nm following the reduction of 0.1 mM 5,5′dithiobis-2-nitrobenzoic acid (ε: 13.6 mL cm^{-1} μmol^{-1}) in the presence of 0.31 mM acetyl-CoA, 0.5 mM oxaloacetic acid, 0.25% Triton X-100, 100 mM Tris-HCl buffer (pH 8.0), and 25 µL retina homogenate in a spectrophotometer cuvette containing a total volume of 1 mL.

The protocol used for evaluating mitochondrial function is presented in Figure 1. Two different states are measured: LEAK respiration represents the nonphosphorylated state in the absence of ADP, and OXPHOS represents oxygen consumption coupled to phosphorylation of ADP to ATP in the presence of saturating ADP. The following substrates and inhibitors were added (final chamber concentration): pyruvate (5 mM), malate (5 mM), ADP (2.5 mM), cytochrome *c* (10 µM), succinate (10 mM), rotenone (1 µM), antimycin A (5 µM), ascorbate (2 mM), tetramethylphenylenediamine (TMPD; 0.5 mM), and sodium azide (100 mM). Pyruvate and malate were added before the retina homogenate and the chamber was closed immediately after homogenate addition. An uncoupler titration (dinitrophenol; 5-µM steps) was performed after succinate in order to determine the maximal capacity of the electron transport system (ETS). Furthermore, addition of digitonin after ADP did not show any increase in respiration, confirming that none of the plasma membranes were left intact after homogenization (results not shown). Mitochondrial respiration was corrected for oxygen flux due to instrumental background, and for residual oxygen consumption (ROX) after inhibition of Complexes I and III, with rotenone and antimycin A, respectively.[35] This protocol provides an indirect assessment of Complex III activity. Although electrons are initially fed into Complexes I, II, or I and II, defects in steps downstream of the Q-cycle, requiring electron transfer by Complexes III and IV, impact the capacity of Complexes I and II. For Complex IV respiration, the chemical background measured in presence of sodium azide was subtracted.

For the detection of qualitative changes in the OXPHOS system, respiration was expressed as flux control ratio (FCR), normalized for maximal OXPHOS capacity in presence of substrates simultaneously feeding electrons into both NADH and succinate pathways (Complex I and II, respectively).

Statistical analyses were performed with SigmaStat 4 (Aspire Software International, Ashburn, VA, USA). Criteria of normality and homogeneity of variance for ANOVA were tested for each variable with Kolmogorov-Smirnov (Lilliefors' correction) and Spearman tests, respectively. For variables meeting the above criteria (FCR, for NADH and succinate pathways; and CS

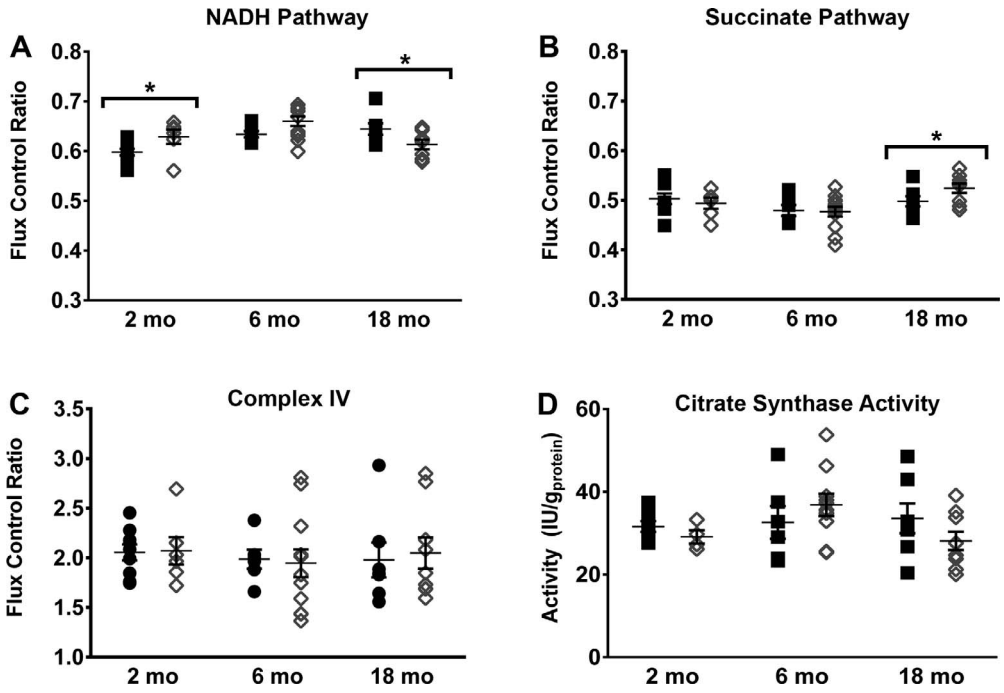

FIGURE 2. Mitochondrial oxidative phosphorylation (OXPHOS) capacity and mitochondrial content in retina homogenates. OXPHOS capacity is expressed as FCR normalized for physiological OXPHOS capacity with substrates feeding electrons into NADH and succinate pathways simultaneously. FCRs are provided for (**A**) NADH pathway (pyruvate+malate+ADP), (**B**) succinate pathway (succinate+rotenone+ADP), and (**C**) Complex IV single step (ascorbate+TMPD+ADP). Finally, (**D**) CS activity (normalized against total protein content in homogenates) is used as an indicator of mitochondrial content. *Asterisks* indicate statistical significance.

activity), differences between age-matched diet groups were tested with 2-way ANOVA, followed by pairwise Tukey comparison. For variables not meeting the criteria (coupling control ratio; FCR for Complex IV; and cytochrome *c* control factor), age-matched differences were analyzed with Mann-Whitney *U* test. Unless otherwise stated, values reported in this study represent mean ± standard error of the mean (SEM). Significance was set to $P < 0.05$.

RESULTS

Changes in Retinal Mitochondrial Respiration Precede T2D

FCR (when normalized for maximal OXPHOS capacity) allows detection of qualitative changes, and this approach revealed a greater NADH pathway contribution to maximal OXPHOS capacity at 2 months (Fig. 2A). At hyperglycemia onset (6 months), no differences were observed; however, statistical comparisons segregating hyperglycemic and hyperinsulinemic status revealed an increase attributed to hyperinsulinemia alone. After sustained hyperglycemia (18 months), NADH pathway FCR was lower in diabetic than in control animals, and this was accompanied by an increased succinate pathway contribution to maximal OXPHOS capacity (Fig. 2B). Statistical comparisons segregating hyperglycemic and hyperinsulinemic status confirmed that this increase was attributed to increases in FBG (18 months).

Regardless of FBG levels, FCR for Complex IV did not vary at any of the time points examined (Fig. 2C). The phosphorylation system did not exert a limitation on electron transport in Nile rat retinas; ratios of maximal OXPHOS/ETS were 0.97 ± 0.03 and 0.96 ± 0.01 in diabetic versus control animals, respectively. Mitochondrial respiratory capacity expressed as a function of tissue mass did not vary between diets (Table 1) and mitochondrial content, as reflected by CS activity, was comparable between age-matched diet groups (Fig. 2D).

Coupling control ratio (LEAK over maximal OXPHOS, below 0.12; Fig. 3A) and stimulation of respiration following addition of ADP (Fig. 1), together demonstrate that mitochondrial electron transport and OXPHOS were well coupled at all ages under our experimental conditions. Coupling control ratio

TABLE 1. Flux Per Mass Values

	2 mo		6 mo		18 mo	
	Prediabetic	Control	Diabetic	Control	Diabetic	Control
LEAK	2.2 ± 0.7	2.8 ± 0.5	4.1 ± 0.6*	2.2 ± 0.7	2.6 ± 0.5	2.2 ± 0.4
NADH pathway	29 ± 5	32 ± 3	36 ± 3	34 ± 4	30 ± 3	29 ± 2
Succinate pathway	22 ± 4	27 ± 3	26 ± 2	26 ± 3	26 ± 3	22 ± 2
NADH–succinate pathway	46 ± 7	54 ± 5	55 ± 4	53 ± 6	49 ± 5	44 ± 3
Maximal COX capacity	96 ± 17	111 ± 11	102 ± 8	104 ± 10	99 ± 10	86 ± 6

COX, cytochrome *c* oxidase.
* $P < 0.05$.

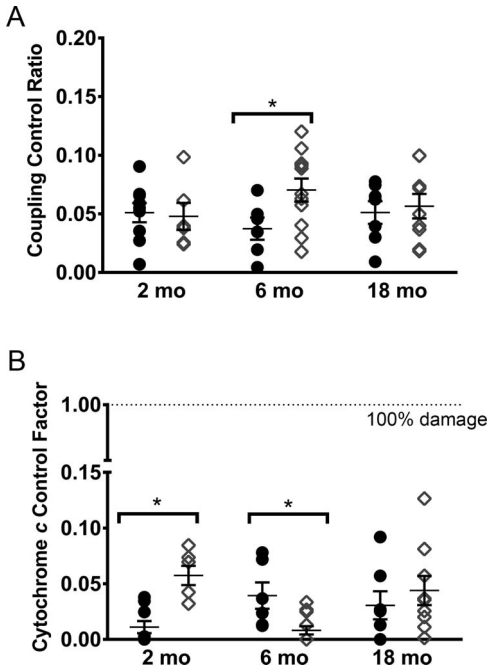

Figure 3. Indicators of coupling and mitochondrial outer membrane integrity. (**A**) Coupling control ratio is expressed as LEAK state over OXPHOS capacity with substrates feeding electrons into NADH and succinate pathways simultaneously. A value of 0.0 indicates fully coupled mitochondria, on a scale of up to 1.0 (representing fully uncoupled mitochondria). (**B**) Mitochondrial outer membrane integrity as the cytochrome *c* control factor, which represents the increase in NADH–OXPHOS capacity pyruvate+malate+ADP due to the addition of exogenous cytochrome *c*. A value of 0.0 indicates full membrane integrity (no loss of endogenous cytochrome *c*), and a value of 1.0 would be complete loss of membrane integrity. *Asterisks* indicate statistical significance.

increases in diabetic animals at 6 months indicated elevated proton leakage and electron slip in the absence of ADP phosphorylation. There were no differences in coupling control ratio at other time points.

Cytochrome *c* control factor was higher in prediabetic (2 months) Nile rats (Fig. 3B). At hyperglycemia onset (6 months), the opposite effect was observed and was still attributed to hyperinsulinemia alone. No differences were detected at 18 months, regardless of insulin or FBG levels.

Type 2 Diabetes

Nile rats fed standard rodent diet progressed from less than 10% of animals (8%) displaying T2D (FBG levels > 5.6 mM) at the first time point examined (2 months), to approximately one-half (44%) demonstrating both elevated FBG and HbA1c by 6 months (Table 2). On this diet, hyperinsulinemia rates doubled from 2 to 6 months (40% to 83%). Hyperinsulinemia declined to 15% at 12 months, with even higher proportions of Nile rats demonstrating elevated FBG (81%) and HbA1c (89%). At the latest time point (18 months) 80% of Nile rats showed a history of hyperglycemia as indicated by elevated HbA1c levels.

Controls never exceeded the threshold for hyperglycemia at any time point. In agreement with maintained normoglycemia at 18 months, controls also exhibited normal HbA1c levels. However, of note, increasing rates of hyperinsulinemia were detected in controls at 6 months (18%), 12 months (38%), and 18 months (62%).

Early Diabetic Retinopathy

The first clinical sign of retinopathy (pericyte loss) is observed in T2D Nile rats from 12 months (Fig. 4A). These animals exhibited a preferential loss of longitudinal pericytes from 12 months onward (12 months: 1481 ± 111 vs. 1746 ± 183, 18 months: 1163 ± 131 vs. 1563 ± 84, in diabetic versus control animals, respectively; Fig. 4B). This corresponds to a 15% ± 3% loss in the total number of longitudinal pericytes at 12 months. The decline in this cell population progressed to 26% ± 4% at 18 months. In contrast, forked pericytes and bridged pericyte cell populations were unaffected. The total pericyte-to-endothelial cell (TP:EC) ratio at 6 months is approximately 1:1 (Fig. 4C) and declines thereafter owing to pericyte loss.

The number of degenerated capillaries was unchanged at 12 months; however, at 18 months there was a >3-fold increase in the number of degenerated capillaries (156 ± 36 in diabetic versus 47 ± 36 in control animals; Fig. 4D).

A second clinical sign of DR demonstrated in diabetic Nile rats is delayed ERG OP kinetics (Fig. 5). OP implicit times were delayed, exclusively under photopic adaptation. Cursor positions on OP base and apex were shifted to longer times, with the exception of two cursors (5 and 6) corresponding to the largest amplitudes in the OP bursts. OP amplitudes were unaffected.

No differences were observed in a- and b-wave amplitudes or implicit times between diabetic and control animals at 18 months, regardless of the adaptation background studied (scotopic, mesopic, or photopic). Finally, b-wave amplitudes were quantified at time 0 versus 10 minutes after switching background adaptation from scotopic to mesopic, as well as from mesopic to photopic, and again no changes were observed.

Table 2. Metabolic Phenotype

	2 mo		6 mo		12 mo		18 mo	
	Control (n = 11)	**Prediabetic (n = 7)**	**Control (n = 10)**	**Diabetic (n = 12)**	**Control (n = 21)**	**Diabetic (n = 20)**	**Control (n = 16)**	**Diabetic (n = 25)**
Body weight, g	66 ± 3	73 ± 3	92 ± 3	98 ± 5	103 ± 3	122 ± 1*	108 ± 3	122 ± 2*
BMI, kg/m^2	5.4 ± 0.2	5.8 ± 0.2	6.9 ± 0.2	7.3 ± 0.3	5.2 ± 0.1	5.9 ± 0.1*	5.5 ± 0.1	5.9 ± 0.1*
FBG, mM	2.9 ± 0.3	2.7 ± 1.4	3.2 ± 1.6	5.4 ± 1.9*	3.8 ± 0.1	10.8 ± 1.1*	3.7 ± 0.2	8.6 ± 1.3*
HbA1c†	N/A	N/A	4.3 ± 0.1	4.1 ± 0.1	4.0 ± 0.1	7.8 ± 0.6*	5.0 ± 0.4	7.7 ± 0.6*
Insulin,‡ ng/mL	0.9 ± 0.3	4.3 ± 1.5*	2.9 ± 1.5	5.6 ± 0.9*	2.2 ± 0.7	0.9 ± 0.3*	2.6 ± 0.6	0.7 ± 0.2*

Data represented as mean ± SEM, Mann-Whitney *U* test. N/A, not applicable.

* $P < 0.05$.

† A subset of animals was used, $n = 4$, 6 (6 months); 4, 8 (12 months), and 4, 10 (18 months); control and diabetic, respectively.

‡ A subset of animals was used, $n = 4$, 5 (2 months); $n = 5$, 9 (6 months); 13, 20 (12 months), and 6, 6 (18 months); control and prediabetic/diabetic, respectively.

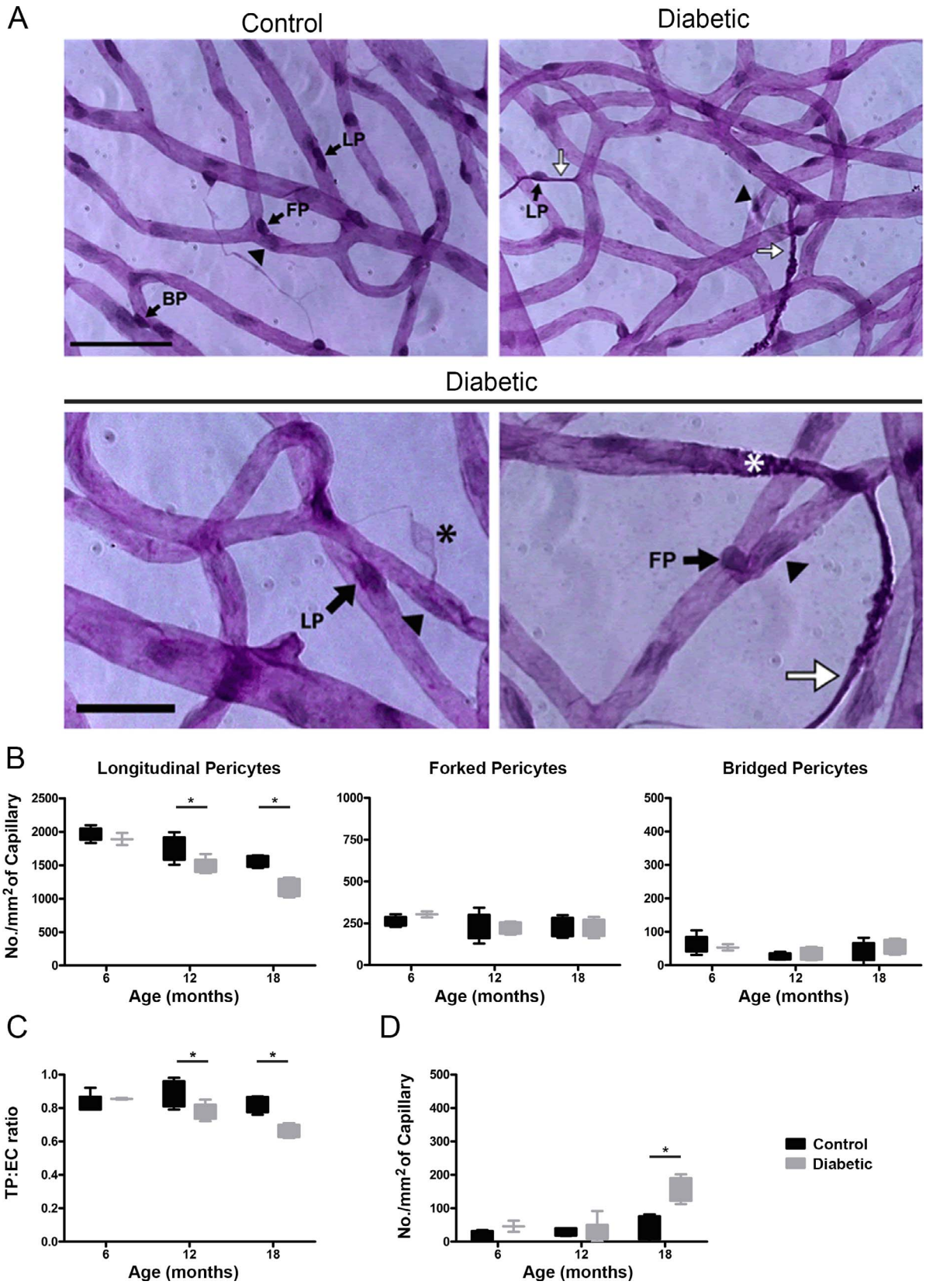

FIGURE 4. Retinal digest preparations of diabetic and control Nile rat retinas. Representative images (**A**) of isolated retinal vasculature, 12 (*lower row*) and 18 months (*upper row*). Quantification of pericyte numbers (**B**), total TP:EC ratio (**C**), and number of degenerated capillaries (**D**). *Scale bar*: 50 μm in *upper panel*; 20 μm, enlarged images in *lower panel*. *Black arrows*: pericytes; *arrowheads*: endothelial cells; *white arrows*: tortuous capillaries; *white asterisk*: early capillary degeneration; *black asterisk*: pericyte ghost. *Asterisks* on graphs indicate statistical significance. LP, longitudinal pericyte; FP, forked pericyte; BP, bridged pericyte.

Investigative Ophthalmology & Visual Science

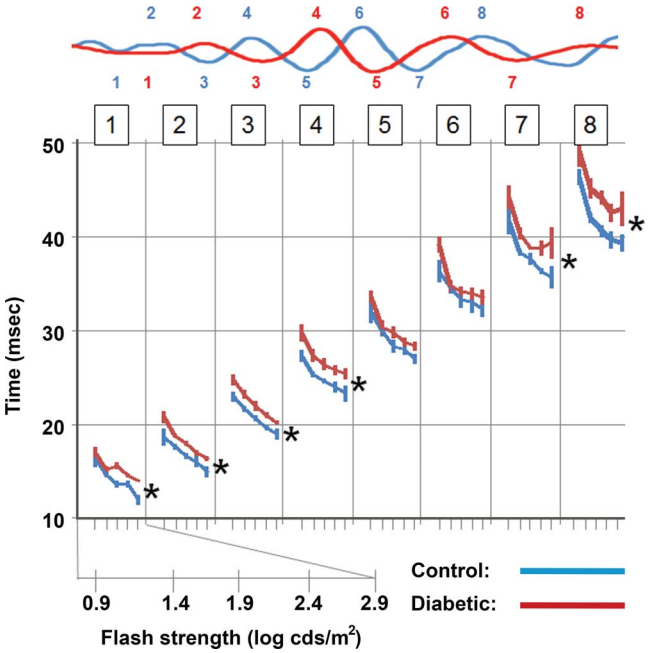

Figure 5. Oscillatory potential timing at 18 months, expressed as a function of stimulus (flash) strength. The *upper panel* shows traces from a diabetic (*red*) and a control (*blue*) in response to the highest strength stimulus (2.9 log cd s/m^2). Timing versus strength graphs are provided separately for each of the eight markers (with the numbers indicated in *upper boxes*). The *x*-axis for the first marker is shown as an inset with strength values for each of the five stimuli presented at incremental strengths (strengths values could not be presented for all eight markers owing to space limitation). *Asterisks* indicate statistical significance.

No evidence of either retinal edema or thinning was observed in diabetic animals from 6 to 18 months at any eccentricity (Fig. 6). ONL and INL measures taken from the central and peripheral retina did not differ between groups (Table 3). Cholinergic amacrine (ChAT-immunoreactive) total cell numbers, both in the INL as well as those displaced in the GCL, were unchanged (Table 3).

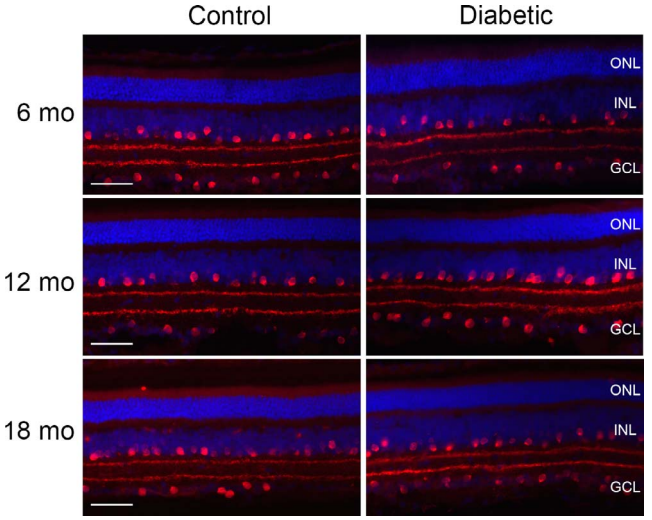

Figure 6. Cross sections of central retina, immunostained for cholinergic amacrine cells (ChAT) in *red* with DAPI-stained nuclei in *blue*. *Scale bar*: 50 μm. ONL, outer nuclear layer.

Table 3. Central and Peripheral Retina Outer and Inner Nuclear Layer Thickness Measures and ChAT-Immunoreactive Amacrine Cell Counts

		6 mo		12 mo		18 mo	
		Control	Diabetic	Control	Diabetic	Control	Diabetic
Center	ONL thickness, μm	29.1 ± 4.9, $n = 4$	30.9 ± 2.9, $n = 3$	28.5 ± 3.5, $n = 6$	30.4 ± 2.8, $n = 6$	28.8 ± 5.0, $n = 6$	29.3 ± 2.8, $n = 6$
	INL thickness, μm	37.6 ± 3.8, $n = 4$	39.5 ± 6.8, $n = 3$	36.8 ± 4.7, $n = 6$	39.5 ± 5.1, $n = 6$	38.8 ± 7.7, $n = 6$	37.1 ± 3.8, $n = 6$
	ChAT+ cells	24 ± 4, $n = 4$	27 ± 4, $n = 3$	28 ± 5, $n = 6$	30 ± 5, $n = 6$	24 ± 5, $n = 4$	29 ± 4, $n = 6$
Periphery	ONL thickness, μm	21.5 ± 3.8, $n = 4$	22.9 ± 2.3, $n = 3$	19.2 ± 2.2, $n = 6$	23.4 ± 1.8, $n = 6$	20.9 ± 3.4, $n = 6$	22.3 ± 2.7, $n = 6$
	INL thickness, μm	25.0 ± 6.8, $n = 4$	23.2 ± 2.2, $n = 3$	22.4 ± 5.9, $n = 6$	25.0 ± 3.6, $n = 6$	26.7 ± 4.7, $n = 6$	27.6 ± 4.2, $n = 6$
	ChAT+ cells	16 ± 4, $n = 4$	18 ± 4, $n = 3$	18 ± 4, $n = 6$	17 ± 3, $n = 6$	20 ± 4, $n = 4$	22 ± 5, $n = 6$

Values indicate average ± standard deviation.

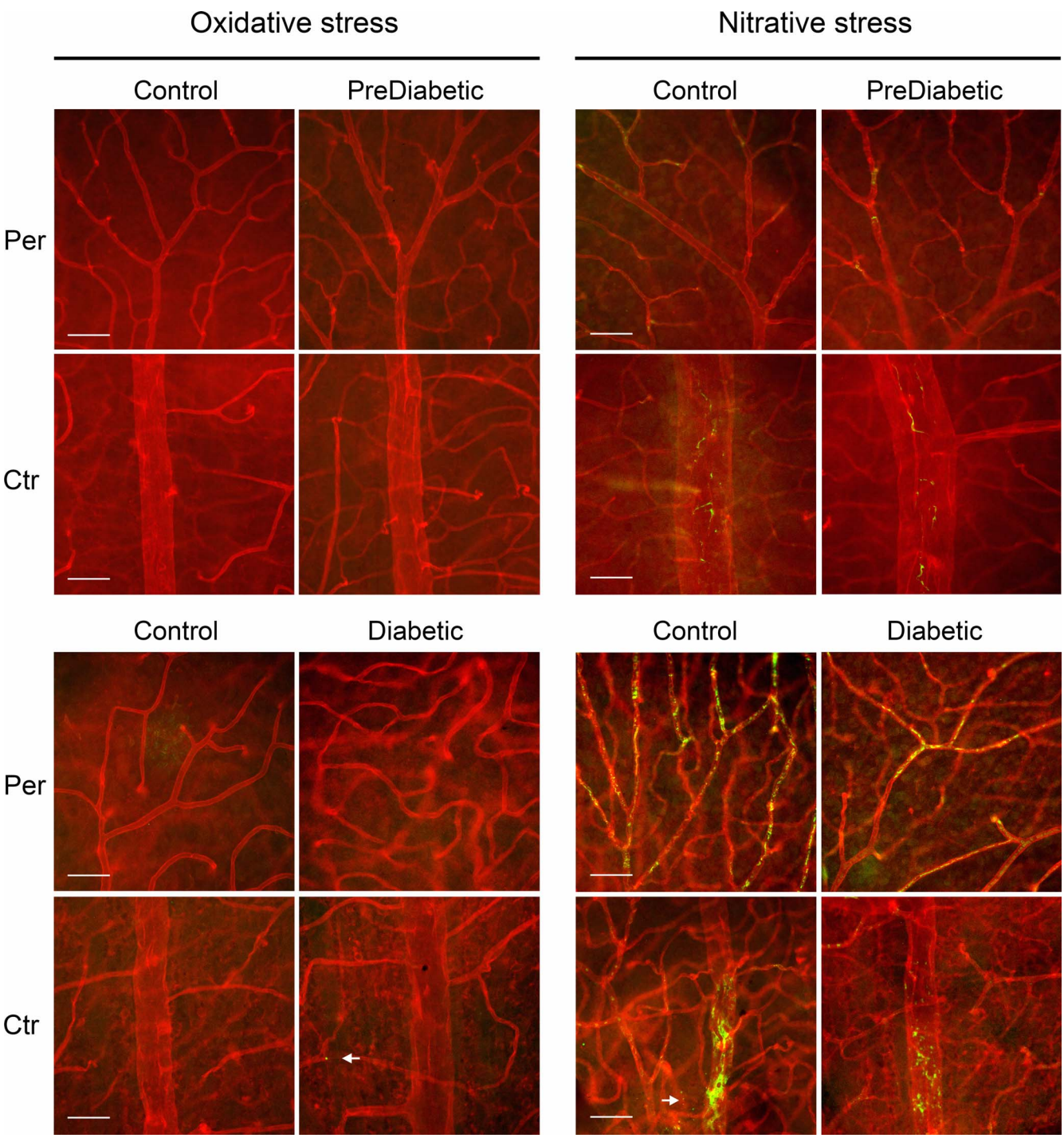

FIGURE 7. Retinal flatmounts of blood vessels (2 months, *top*; 12 months, *bottom*) stained for oxidative (4-hydroxynonenal) and nitrative (nitrotyrosine) stress in *green*. Tomato lectin staining of vasculature in *red*. Extravascular immunoreactivity for stress markers (*white arrows*). *Scale bar*: 50 μm. Ctr, center; Per, periphery.

Likewise, no differences were detected in retinal flatmounts stained with specific oxidative/nitrative stress markers (Fig. 7). Very low levels of extravascular lipid oxidative modifications were demonstrated with 4-hydroxynonenal–specific antibodies (12 months only); the retinal vasculature was devoid of any detectable immunoreactivity. The nitrative stress marker nitrotyrosine was detected at low levels in blood vessels of both groups at 2 months. This vascular staining was exacerbated at 12 months in both central and peripheral retina but did not differ between groups.

Cataracts of Increasing Severity

Fluorescein angiography (FA) was performed to assess inner retinal vasculature. Imaging of diabetic animals was limited owing to impedance by cataract formation. Clearly evident in the eyes of diabetic animals (Fig. 8A; Fig. 8B, lens only), cataracts exhibited a range of severity (Figs. 8C–I), illustrating the barrier to examining retinal blood vessels in vivo (Figs. 8D–J). Incidence increased from 13% at 12 months, to 50% at 18 months. Cataracts were never detected in controls at any of the

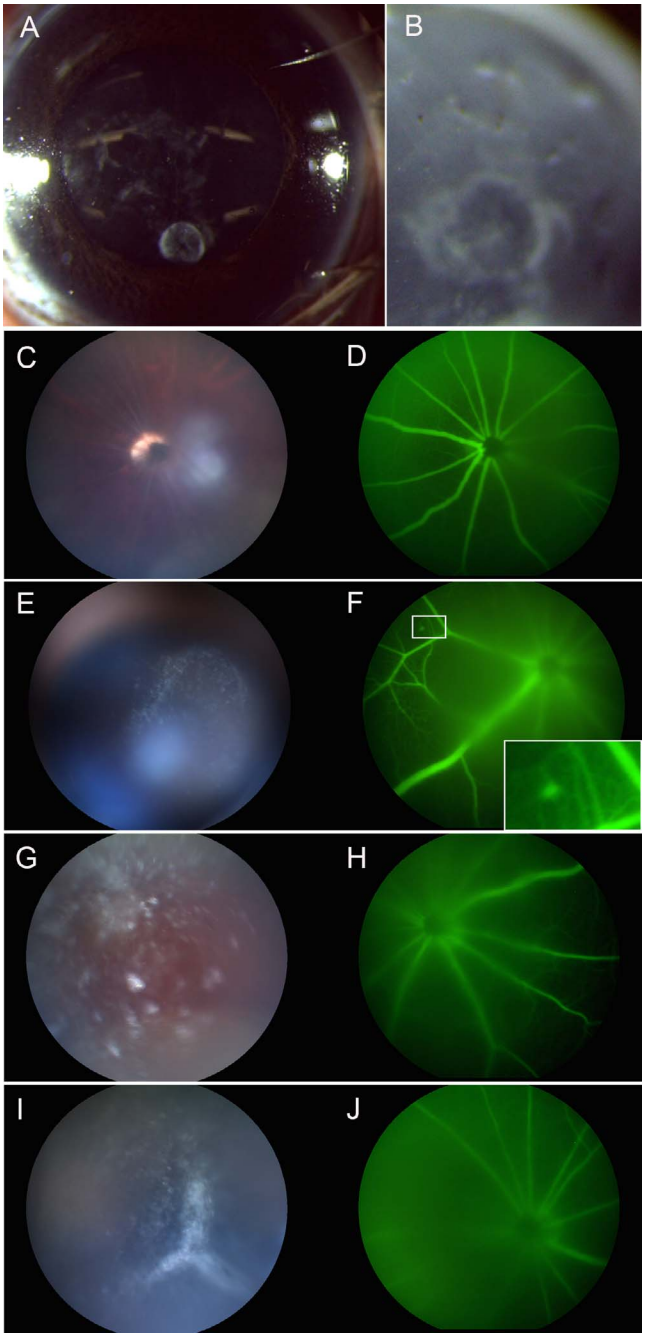

FIGURE 8. Example of cataractogenesis in 18-month hyperglycemic Nile rats. Enucleated eye (**A**) with isolated lens (**B**). Representative fundus images of increasing cataract severity (**C**, **E**, **G**, **I**) with corresponding fluorescein angiography image (**D**, **F**, **H**, **J**). Inset in (**F**) demonstrates a microaneurysm.

ages examined. Although, rarely observed, evidence of a microaneurysm in an 18-month diabetic Nile rat is presented in Figure 8F (inset).

DISCUSSION

The present study established that high-resolution respirometry (with a multiple substrate-inhibitor-titration protocol to assess individual respiratory Complex function) can be applied to isolated retinas. Furthermore, unlike the other approaches such as Seahorse,[36] high-resolution respirometry allows the normalization of results as FCR values, which is crucial to accurately detect modest changes, and also allows many titration protocols to be performed in a single experiment. We showed evidence of well-coupled mitochondria in tissue homogenates, which allowed us to identify changes in oxidative phosphorylation and breaches in outer membrane integrity during insulin resistance (2 months), before the manifestation of hyperglycemia (6 months), in *Arvicanthis niloticus* (Nile rat). In addition, we provided evidence of delayed OPs (specific to the cone pathway) and increased incidence of cataractogenesis after prolonged hyperglycemia in retinas of this cone-rich diurnal rodent model, which recapitulates the five stages of human T2D progression[18] (Fig. 9). A key target in the development of DR is the synergistic interaction between neurons (amacrine and retinal ganglion cells), glial cells (Müller cells and astrocytes), and blood vessels (endothelial cells and pericytes) involved in the autoregulation of vascular flow and metabolic activity.[37] Dysregulation of this "neurovascular unit" has been implicated in diabetes, in part due to oxidative stress originating from the outer retina,[8] and well before onset of clinically detectable DR.[38] According to Kooragayala et al.,[36] photoreceptors have limited mitochondrial reserve capacity for ATP production from their electron transport system. Therefore, photoreceptors are particularly vulnerable to changes in homeostasis. Fort et al.[39] have observed that during the initial stages of type 1 diabetes, the retina compensates by lowering its constitutively high metabolic activity. Reductions in retinal electrical activity,[40] biosynthetic activity,[41] increases in autophagic flux in the outer plexiform layer,[42] and even apoptosis of marginal populations of neural and vascular cells[43] are all contributors. However, these mechanisms eventually fail, leading to the first clinically detectable signs of DR, specific to inner retina microvasculature: capillary basement membrane thickening and pericyte loss. Our results support that changes in mitochondrial function and integrity occur early and likely contribute to transient compensation in an attempt to maintain energy homeostasis.

Increased respiration at 2 months, as a result of exogenous cytochrome *c* entering the intermembrane space, indicates changes in mitochondrial membrane properties (such as composition and/or organization). Surprisingly, this transient increase in outer membrane permeability was associated with an increase in NADH pathway (Complex I and related dehydrogenases) contribution to maximal OXPHOS capacity, whereas it is generally associated with defects in mitochondrial respiratory complexes.[20,44] At the onset of hyperglycemia (6 months), we observed increases in LEAK and decreases in cytochrome *c* access to mitochondrial respiratory complexes without paradoxical increases in NADH pathway activity. One possible explanation would be that early changes in mitochondrial function and integrity might entice transient compensation for the maintenance of energy homeostasis. Changes in mitochondrial membrane composition take several months to develop[45–47] and may explain the improved membrane integrity observed in 6-month diabetic animals, with no further changes at 18 months.

Mitochondria were well coupled in prediabetic animals, without decreased respiratory capacity, emphasizing the specificity of this change in membrane sensitivity in retinal mitochondria. These early changes did not correlate with fasting plasma insulin levels. Increased mitochondrial membrane permeability was documented in isolated mitochondria from retinas of Zucker diabetic fatty (ZDF) rats during hyperinsulinemia (before hyperglycemia), but alongside a decrease (rather than an increase) in Complex III activity.[48] Decreases in Complex III activity (without changes in Complex

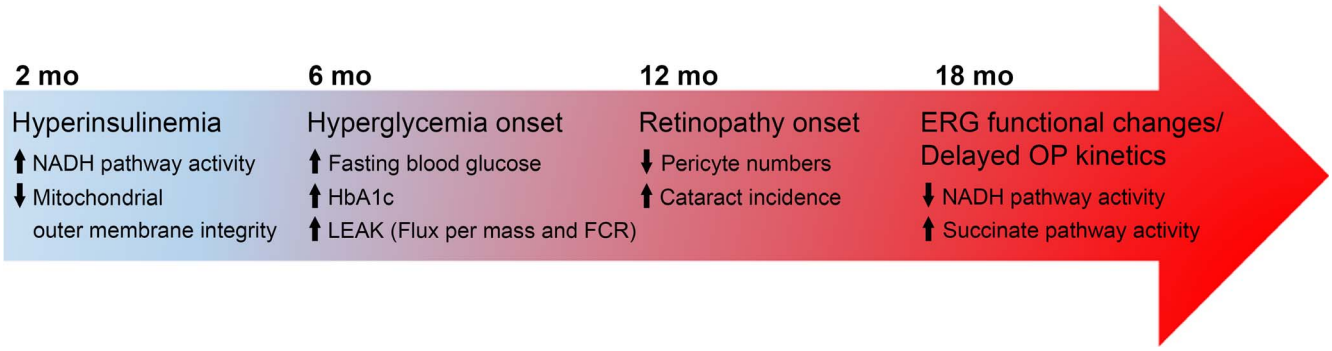

Figure 9. Timeline of events as a function of age and type 2 diabetes and associated retinopathy progression in Nile rats.

I) were also reported in STZ mice.[49] Respiration in the presence of substrates feeding electrons into Complex I (NADH pathway), II (succinate pathway), or I and II also involves Complexes III and IV, and so a decrease in Complex III would cause a decrease in maximal OXPHOS capacity, which was not observed in our study. The above differences between animal models epitomizes the debate about whether changes in mitochondrial capacity are causal or consequential to insulin resistance.[28,50,51] Such discrepancies between models and studies might in fact provide pertinent insight into the intricate relationship between mitochondria and insulin action, and subsequently effective preventative targets.

Enhanced NADH pathway contribution to maximal OXPHOS capacity in retinas is reminiscent of data on cardiac mitochondria showing an increase in mitochondrial oxidation of palmitoyl carnitine, glutamate, and succinate in insulin-resistant mice,[51] and an increase in oxidation of palmitoyl-CoA and octanoylcarnitine, as well as in Complex I activity, at early stages of diabetes in fructose-fed rats.[52] Complexes I, II, and III have the highest capacity for superoxide production[53]; therefore, decreases in their activity (albeit associated with maintenance of respiratory complex flux) would lead to excessive free radical production. In fact, most mitochondria produce superoxide high rates after addition of the Complex I inhibitor rotenone,[53,54] and furthermore, several pathologies involving defects in Complex I are associated with elevated production of superoxide.[55,56] Therefore, the initial increase in relative contribution of electron flow through Complex I observed during prediabetes (2 months) could represent a compensatory mechanism serving to reduce the production of ROS. In contrast, at 18 months of age, after 1 year of hyperglycemia, reduced NADH pathway capacity suggests pathology as a result of oxidative stress. However, the age-related changes previously reported in other tissues (reduced CS activity and decrease in the activity of mitochondrial complexes)[57,58] were not observed in Nile rat retinas at 18 months, regardless of their diabetic status. We failed to detect upregulation of targeted oxidative/nitrative stress markers in retinal vasculature of either prediabetic (2 months) or diabetic animals (up to 12 months) relative to controls. Our main focus with limited starting material was to examine the vasculature for 4-HNE (marker of aldehydic products of lipid peroxidation) and nitrotyrosine formation, specifically as a possible cause of pericyte dropout, using an approach that successfully demonstrated upregulation of oxidative/nitrative stress in whole-mounted retinas (STZ rat model).[59] Our high-resolution respirometry results support these findings. We cannot rule out that examination of additional markers (and/or later time points) may have demonstrated oxidative stress in the vasculature. Assuming that oxidative stress would have occurred in the retina, then the expected outcome would have been a decrease (and not an increase as observed here) in NADH pathway activity.[53–56] In STZ rats, at early stages (1–3 weeks post induction) retinal mitochondria have been shown to undergo adaptive changes associated with maintained energetic requirements and prevention of oxidative stress.[60] However, at later stages (after 8–12 weeks post induction), upregulation of oxidative stress markers was reported.[59] STZ rats are characterized by hyperglycemia due to insufficient insulin secretion (T1D model), whereas Nile rats undergo hyperinsulinemia without initial hyperglycemia (T2D model). While STZ studies show adaptive mitochondrial changes at early stages of hyperglycemia (without elevated insulin levels), the mitochondrial changes reported here in Nile rats precede manifestations of DR.

Well-established clinical indicators of early DR, oscillatory potentials,[61–63] were affected at 18 months in diabetic Nile rats; implicit times were prolonged while amplitudes were preserved. Of interest, Morlet wavelet transform failed to detect implicit time delays in this study. Morlet is limited to time domain analysis of the largest amplitude oscillatory components and these OPs were not delayed. Similar findings were reported in early human DR and in animal models where delays in OPs also preceded changes in their amplitudes.[64,65] Using a mouse model of T2D (high-fat diet), Rajagopal et al.[66] have reported delayed OP timing as the first functional retinal phenotype, coinciding with the peak of insulin resistance (6 months). Once hyperglycemia develops (by 12 months), amplitudes become reduced, alongside microvascular changes. However, a- and b-waves (amplitudes and latencies) are unaltered,[66] as was the case in diabetic Nile rats. Our findings support previous evidence that changes in OPs precede those in b-waves.[67] One major difference with mouse and rat models is that alterations in OPs in these nocturnal rodents were detected under scotopic adaptation. Interestingly, we only observed alterations in OPs when recorded under photopic adaptation, which could be related to the higher proportion of cones in Nile rats (35%)[68] compared to rats and mice (1%–3%).[69,70] Our observation of preserved OP amplitudes is in agreement with the preserved total number of cholinergic amacrine cells, which likely contribute to OP generation together with other inner retina neurons.[71] Studies in induced and spontaneous diabetes type 1 diabetic rodent models (STZ rats and $Ins2^{Akita}$ mice, respectively) report the loss of both cholinergic and dopaminergic amacrine cells; however, ERG recordings have not been performed.[72] Other studies on STZ models have reported defects in a-waves, but whether these reflect impaired photoreceptoral response to light due to hyperglycemia[73] or a direct toxic effect of STZ[74] remains unclear. Our ERG results therefore further support that DR is at its earliest stage of manifestation in Nile rats. The lack of changes in a-wave amplitudes and implicit times in our study implies that changes in photoreceptor metabolism likely

contribute to DR initiation,[8] without early concomitant changes in photoreceptor response to light flashes.

The 50% incidence of cataracts in diabetic Nile rats, at this time point, is similar to the high incidence reported in T2D patients.[75]

Pericyte loss was preferential to the subtype lining straight capillaries as previously reported in the $Ins2^{Akita}$ mouse model of type 1 diabetes,[76] as opposed to pericytes lining forked capillaries or bridging adjacent capillaries. While the underlying mechanisms elude us, one avenue warranting scrutiny is the potential for hyperglycemia to alter the types of integrins expressed on specific pericytes, and hence modulate their response to pro-apoptotic ligands such as angiopoietin-2.[77] Recent in vitro studies by Zhang et al.[78] have demonstrated increased levels of autoantibodies against pericyte cell surface antigens in the serum of DR patients. Of interest in terms of the Nile rat's pertinence as a DR model, the ratio of total pericytes over endothelial cells (at 6 months, before any cell loss) was close to 1:1, as observed in humans,[79] which contrasts with the 1:3 ratio reported in rats.[80] Degenerated capillaries were only observed at the latest time point (18 months), consistent with DR progression.[3–6]

Control animals did not become hyperglycemic up to 18 months, but they did demonstrate hyperinsulinemia from 6 months onward, which alone is not associated with DR. Harris and colleagues[74] have estimated that T2D likely develops over 12 years (and retinopathy over 7 years) before a clinical diagnosis of T2D. Our results from high-resolution respirometry support that early mitochondrial function changes might be part of these insidious changes that precede clinical detection of T2D and therefore, DR.

One major limitation to characterizing retinal mitochondrial change during the development of diabetes (and other insults) is the limited amount of tissue. Examples of specific changes that could not be directly assessed in our broad-scope study include (1) complementary assays to measure oxidative stress directly in isolated mitochondria; (2) specific content analysis of mitochondrial external membranes (such as phospholipid types and cardiolipin); and (3) direct measures of Complex III activity, using spectrophotometric assay for this protein. Although indirect, our overall data did not support a potential defect in Complex III.

Conclusions

There is overwhelming experimental evidence linking hyperglycemia with pericyte loss and development of microvascular complications in early DR.[43] Application of high-resolution respirometry, with a multiple substrate-inhibitor-titration protocol, allowed detection of early-onset retinal changes in the Nile rat T2D model. Hyperinsulinemia is associated with increased contribution of NADH pathway to oxidative phosphorylation and with compromised outer membrane integrity. The diet-based difference between groups is of particular relevance, as it offers the potential to mimic clinical interventions aimed at reversing hyperglycemia itself, such as with diet or metformin. A key challenge is to understand why in some patients, even with hyperglycemia reversal, progression to retinopathy continues. This model would be a valuable tool to examine whether hyperinsulinemia alone might "program" retinopathy onset.

Acknowledgments

The authors thank Zhining Zhu for her diligent care of our Nile rat colony, Rachel Bryant for Nile rat handling, and Jillian Schneider for helping WHH with oxygraph experiments.

Supported by Canadian Institutes of Health (CIHR; MOP 125873) to YS and CBC; YS is an AHFMR Senior Scholar (200800242); JG received a scholarship from the Alberta Diabetes Institute. WHH received a scholarship from the University of Alberta Faculty of Medicine and Dentistry 75th anniversary. HH received a scholarship from the China Scholarship Council.

Disclosure: **W.H. Han**, None; **J. Gotzmann**, None; **S. Kuny**, None; **H. Huang**, None; **C.B. Chan**, None; **H. Lemieux**, None; **Y. Sauvé**, None

References

1. International Diabetes Federation. *IDF Diabetes*. 7th ed. Brussels, Belgium: International Diabetes Federation; 2015. Available at: http://www.diabetesatlas.org. Accessed July 20, 2017.
2. Chen L, Magliano DJ, Zimmet PZ. The worldwide epidemiology of type 2 diabetes mellitus—present and future perspectives. *Nat Rev Endocrinol*. 2011;8:228–236.
3. Bianchi E, Ripandelli G, Taurone S, et al. Age and diabetes related changes of the retinal capillaries: an ultrastructural and immunohistochemical study. *Int J Immunopathol Pharmacol*. 2016;29:40–53.
4. Warmke N, Griffin KJ, Cubbon RM. Pericytes in diabetes-associated vascular disease. *J Diabetes Complications*. 2016; 30:1643–1650.
5. Zhang W, Liu H, Al-Shabrawey M, Caldwell RW, Caldwell RB. Inflammation and diabetic retinal microvascular complications. *J Cardiovasc Dis Res*. 2011;2:96–103.
6. Stitt AW, Curtis TM, Chen M, et al. The progress in understanding and treatment of diabetic retinopathy. *Prog Retin Eye Res*. 2016;51:156–186.
7. Moran EP, Wang Z, Chen J, Sapieha P, Smith LE, Ma JX. Neurovascular cross talk in diabetic retinopathy: pathophysiological roles and therapeutic implications. *Am J Physiol Heart Circ Physiol*. 2016;311:H738–H749.
8. Du Y, Veenstra A, Palczewski K, Kern TS. Photoreceptor cells are major contributors to diabetes-induced oxidative stress and local inflammation in the retina. *Proc Natl Acad Sci U S A*. 2013;110:16586–16591.
9. Tonade D, Liu H, Kern TS. Photoreceptor cells produce inflammatory mediators that contribute to endothelial cell death in diabetes. *Invest Ophthalmol Vis Sci*. 2016;57:4264–4271.
10. Okawa H, Sampath AP, Laughlin SB, Fain GL. ATP consumption by mammalian rod photoreceptors in darkness and in light. *Curr Biol*. 2008;18:1917–1921.
11. Prunty MC, Aung MH, Hanif AM, et al. In vivo imaging of retinal oxidative stress using a reactive oxygen species-activated fluorescent probe. *Invest Ophthalmol Vis Sci*. 2015;56:5862–5870.
12. Rueda EM, Johnson JE Jr, Giddabasappa A, et al. The cellular and compartmental profile of mouse retinal glycolysis, tricarboxylic acid cycle, oxidative phosphorylation, and ~P transferring kinases. *Mol Vis*. 2016;22:847–885.
13. Robinson R, Barathi VA, Chaurasia SS, Wong TY, Kern TS. Update on animal models of diabetic retinopathy: from molecular approaches to mice and higher mammals. *Dis Model Mech*. 2012;5:444–456.
14. Ramos D, Carretero A, Navarro M, et al. Mimicking microvascular alterations of human diabetic retinopathy: a challenge for the mouse models. *Curr Med Chem*. 2013;20: 3200–3217.
15. Cai X, McGinnis JF. Diabetic retinopathy: animal models, therapies, and perspectives. *J Diabetes Res*. 2016;2016: 3789217.

16. Chaabo F, Pronczuk A, Maslova E, Hayes K. Nutritional correlates and dynamics of diabetes in the Nile rat (Arvicanthis niloticus): a novel model for diet-induced type 2 diabetes and the metabolic syndrome. *Nutr Metab (Lond)*. 2010;7:29.
17. Noda K, Melhorn MI, Zandi S, et al. An animal model of spontaneous metabolic syndrome: Nile grass rat. *FASEB J*. 2010;24:2443–2453.
18. Yang K, Gotzmann J, Kuny S, Huang H, Sauvé Y, Chan CB. Five stages of progressive β-cell dysfunction in the laboratory Nile rat model of type 2 diabetes. *J Endocrinol*. 2016;229:343–356.
19. Noda K, Nakao S, Zandi S, Sun D, Hayes KC, Hafezi-Moghadam A. Retinopathy in a novel model of metabolic syndrome and type 2 diabetes: new insight on the inflammatory paradigm. *FASEB J*. 2014;28:2038–2046.
20. Gilmour GS, Gaillard F, Watson J, et al. The electroretinogram (ERG) of a diurnal cone-rich laboratory rodent, the Nile grass rat (Arvicanthis niloticus). *Vision Res*. 2008;8:2723–2731.
21. Gaillard F, Bonfield S, Gilmour GS, et al. Retinal anatomy and visual performance in a diurnal cone-rich laboratory rodent, the Nile grass rat (Arvicanthis niloticus). *J Comp Neurol*. 2008;510:525–538.
22. Saïdi T, Mbarek S, Chaouacha-Chekir RB, Hicks D. Diurnal rodents as animal models of human central vision: characterisation of the retina of the sand rat Psammomys obsesus. *Graefes Arch Clin Exp Ophthalmol*. 2011;249:1029–1037.
23. Wang Q, Tikhonenko M, Bozack SN, et al. Changes in the daily rhythm of lipid metabolism in the diabetic retina. *PLoS One*. 2014;9:e95028.
24. Cheung CY, Ikram MK, Klein R, Wong TY. The clinical implications of recent studies on the structure and function of the retinal microvasculature in diabetes. *Diabetologia*. 2015;58:871–885.
25. Hajmousa G, Elorza AA, Nies VJ, Jensen EL, Nagy RA, Harmsen MC. Hyperglycemia induces bioenergetic changes in adipose-derived stromal cells while their pericytic function is retained. *Stem Cells Dev*. 2016;25:1444–1453.
26. Bhatti JS, Bhatti GK, Reddy PH. Mitochondrial dysfunction and oxidative stress in metabolic disorders: a step towards mitochondria based therapeutic strategies. *Biochim Biophys Acta*. 2017;1863:1066–1077.
27. Patti ME, Corvera S. The role of mitochondria in the pathogenesis of type 2 diabetes. *Endocr Rev*. 2010;31:364–395.
28. Sivitz WI, Yorek MA. Mitochondrial dysfunction in diabetes: from molecular mechanisms to functional significance and therapeutic opportunities. *Antioxid Redox Signal*. 2010;12:537–577.
29. Montgomery MK, Turner N. Mitochondrial dysfunction and insulin resistance: an update. *Endocr Connect*. 2015;4:R1–R15.
30. Zhong Q, Kowluru RA. Diabetic retinopathy and damage to mitochondrial structure and transport machinery. *Invest Ophthalmol Vis Sci*. 2011;52:8739–8746.
31. Saudek CD, Herman WH, Sacks DB, Bergenstal RM, Edelman D, Davidson MB. A new look at screening and diagnosing diabetes mellitus. *J Clin Endocrinol Metab*. 2008;93:2447–2453.
32. Dietrich N, Hammes HP. Retinal digest preparation: a method to study diabetic retinopathy. *Methods Mol Biol*. 2012;933:291–302.
33. Gnaiger E. Oxygen calibration by DatLab. *Mitochondr Physiol Network*. 2016;19.18:39–48.
34. Kuznetsov AV, Schneeberger S, Seiler R, et al. Mitochondrial defects and heterogeneous cytochrome *c* release after cardiac cold ischemia and reperfusion. *Am J Physiol Heart Circ Physiol*. 2004;286:H1633–H1641.
35. Gnaiger E, Lassnig B, Kuznetsov A, Reiger G, Margreiter R. Mitochondrial oxygen affinity, respiratory flux control and excess capacity of cytochrome *c* oxidase. *J Exp Biol*. 1998;201:1129–1139.
36. Kooragayala K, Gotoh N, Cogliati T, et al. Quantification of oxygen consumption in retina ex vivo demonstrates limited reserve capacity of photoreceptor mitochondria. *Invest Ophthalmol Vis Sci*. 2015;56:8428–8436.
37. Metea MR, Newman EA. Signalling within the neurovascular unit in the mammalian retina. *Exp Physiol*. 2007;92:635–640.
38. Lott ME, Slocomb JE, Shivkumar V, et al. Comparison of retinal vasodilator and constrictor responses in type 2 diabetes. *Acta Ophthalmol*. 2012;90:e434–e441.
39. Fort PE, Losiewicz MK, Pennathur S, et al. mTORC1-independent reduction of retinal protein synthesis in type 1 diabetes. *Diabetes*. 2014;63:3077–3090.
40. Harrison WW, Bearse MA Jr, Ng JS, et al. Multifocal electroretinograms predict onset of diabetic retinopathy in adult patients with diabetes. *Invest Ophthalmol Vis Sci*. 2011;52:772–777.
41. Gardner TW, Abcouwer SF, Losiewicz MK, Fort PE. Phosphatase control of 4E-BP1 phosphorylation state is central for glycolytic regulation of retinal protein synthesis. *Am J Physiol Endocrinol Metab*. 2015;309:E546–E556.
42. Piano I, Novelli E, Della Santina L, et al. Involvement of autophagic pathway in the progression of retinal degeneration in a mouse model of diabetes. *Front Cell Neurosci*. 2016;10:42.
43. Barber AJ, Gardner TW, Abcouwer SF. The significance of vascular and neural apoptosis to the pathology of diabetic retinopathy. *Invest Ophthalmol Vis Sci*. 2011;52:1156–1163.
44. Toleikis A, Trumbeckaite S, Majiene D. Cytochrome *c* effect on respiration of heart mitochondria: influence of various factors. *Biosci Rep*. 2005;25:387–397.
45. Lemieux H, Blier PU, Tardif JC. Does membrane fatty acid composition modulate mitochondrial functions and their thermal sensitivities? *Comp Biochem Physiol A Mol Integr Physiol*. 2008;149:20–29.
46. Sullivan EM, Fix A, Crouch MJ, et al. Murine diet-induced obesity remodels cardiac and liver mitochondrial phospholipid acyl chains with differential effects on respiratory enzyme activity. *J Nutr Biochem*. 2017;45:94–103.
47. Hoeks J, de Wilde J, Hulshof MFM, et al. High fat diet-induced changes in mouse muscle mitochondrial phospholipids do not impair mitochondrial respiration despite insulin resistance. *PLoS One*. 2011;6:e27274.
48. Kowluru RA, Mishra M, Kowluru A, Kumar B. Hyperlipidemia and the development of diabetic retinopathy: comparison between type 1 and type 2 animal models. *Metabolism*. 2016;65:1570–1581.
49. Kanwar M, Chan PS, Kern TS, Kowluru RA. Oxidative damage in the retinal mitochondria of diabetic mice: possible protection by superoxide dismutase. *Invest Ophthalmol Vis Sci*. 2007;48:3805–3811.
50. Murrow BA, Hoehn KL. Mitochondrial regulation of insulin action. *Int J Biochem Cell Biol*. 2010;42:1936–1939.
51. Gupte AA, Minze LJ, Reyes M, et al. High-fat feeding-induced hyperinsulinemia increases cardiac glucose uptake and mitochondrial function despite peripheral insulin resistance. *Endocrinology*. 2013;154:2650–2662.
52. Lou P-H, Lucchinetti E, Scott K, et al. Dysfucntional fatty acid oxidation and sirtuin signaling characterize early type-2 diabetic hearts of fructose-fed rat. *Am J Physiol*. 2017. In press.
53. Brand MD. The sites and topology of mitochondrial superoxide production. *Exp Gerontol*. 2010;45:466–472.

Investigative Ophthalmology & Visual Science

54. Radad K, Rausch WD, Gille G. Rotenone induces cell death in primary dopaminergic culture by increasing ROS production and inhibiting mitochondrial respiration. *Neurochem Int*. 2006;49:379–386.
55. Raha S, Robinson BH. Mitochondria, oxygen free radicals, disease and aging. *Trends Biochem Sci*. 2000;25:502–508.
56. Pitkanen S, Robinson BH. Mitochondrial complex I deficiency leads to increased production of superoxide radicals and induction of superoxide dismutase. *J Clin Invest*. 1996;98:345–351.
57. Lesnefsky EJ, Chen Q, Hoppel CL. Mitochondrial metabolism in aging heart. *Circ Res*. 2016;118:1593–1611.
58. Rosca MG, Lemieux H, Hoppel CL. Mitochondria in the elderly: is acetylcarnitine a rejuvenator? *Adv Drug Deliv Rev*. 2009;61:1332–1342.
59. Lamoke F, Shaw S, Yuan J, et al. Increased oxidative and nitrative stress accelerates aging of the retinal vasculature in the diabetic retina. *PLoS One*. 2015;10:e0139664.
60. Osorio-Paz I, Uribe-Carvajal S, Salceda R. In the early stages of diabetes, rat retinal mitochondria undergo mild uncoupling due to UCP2 activity. *PLoS One*. 2015;10:e0122727.
61. Yonemura D, Aoki T, Tsuzuki K. Electroretinogram in diabetic retinopathy. *Arch Ophthalmol*. 1962;68:19–24.
62. Tzekov R, Arden GB. The electroretinogram in diabetic retinopathy. *Surv Ophthalmol*. 1999;44:53–60.
63. Pescosolido N, Barbato A, Stefanucci A, Buomprisco G. Role of electrophysiology in the early diagnosis and follow-up of diabetic retinopathy. *J Diabetes Res*. 2015;2015:319692.
64. Shirao Y, Kawasaki K. Electrical responses from diabetic retina. *Prog Retin Eye Res*. 1998;17:59–76.
65. Kizawa J, Machida S, Kobayashi T, Gotoh Y, Kurosaka D. Changes of oscillatory potentials and photopic negative response in patients with early diabetic retinopathy. *Jpn J Ophthalmol*. 2006;50:367–373.
66. Rajagopal R, Bligard GW, Zhang S, Yin L, Lukasiewicz P, Semenkovich CF. Functional deficits precede structural lesions in mice with high-fat diet-induced diabetic retinopathy. *Diabetes*. 2016;65:1072–1084.
67. Layton CJ, Safa R, Osborne NN. Oscillatory potentials and the b-Wave: partial masking and interdependence in dark adaptation and diabetes in the rat. *Graefes Arch Clin Exp Ophthalmol*. 2007;245:1335–1345.
68. Szél A, Röhlich P. Two cone types of rat retina detected by anti-visual pigment antibodies. *Exp Eye Res*. 1992;55:47–52.
69. Szél A, Röhlich P, Caffé AR, Juliusson B, Aguirre G, Van Veen T. Unique topographic separation of two spectral classes of cones in the mouse retina. *J Comp Neurol*. 1992;325:327–342.
70. Petit-Jacques J, Völgyi B, Rudy B, Bloomfield S. Spontaneous oscillatory activity of starburst amacrine cells in the mouse retina. *J Neurophysiol*. 2005;94:1770–1780.
71. Gastinger MJ, Singh RS, Barber AJ. Loss of cholinergic and dopaminergic amacrine cells in streptozotocin-diabetic rat and Ins2Akita-diabetic mouse retinas. *Invest Ophthalmol Vis Sci*. 2006;47:3143–3150.
72. Ottlecz A, Garcia CA, Eichberg J, Fox DA. Alterations in retinal Na+, K(+)-ATPase in diabetes: streptozotocin-induced and Zucker diabetic fatty rats. *Curr Eye Res*. 1993;12:1111–1121.
73. Park SH, Park JW, Park SJ, et al. Apoptotic death of photoreceptors in the streptozotocin-induced diabetic rat retina. *Diabetologia*. 2003;46:1260–1268.
74. Harris MI, Klein R, Welborn TA, Knuiman MW. Onset of NIDDM occurs at least 4-7 yr before clinical diagnosis. *Diabetes Care*. 1992;15:815–819.
75. Li L, Wan XH, Zhao GH. Meta-analysis of the risk of cataract in type 2 diabetes. *BMC Ophthalmol*. 2014;14:94.
76. Pfister F, Feng Y, Hagen F, et al. A novel mechanism of pericyte loss in experimental diabetic retinopathy. *Diabetes*. 2008;57:2495–2502
77. Park SW, Yun JH, Kim JH, Kim KW, Cho CH, Kim JH. Angiopoietin 2 induces pericyte apoptosis via α3β1 integrin signaling in diabetic retinopathy. *Diabetes*. 2014;63:3057–3068.
78. Zhang L, Li Y, Payne J, et al. Presence of retinal pericyte-reactive autoantibodies in diabetic retinopathy patients. *Sci Rep*. 2016;6:20341.
79. Cogan DG, Kuwabara T. The mural cell in perspective. *Arch Ophthalmol*. 1967;78:133–143.
80. Tilton RG, Miller EJ, Kilo C, Williamson JR. Pericyte form and distribution rat retinal and uveal capillaries. *Invest Ophthalmol Vis Sci*. 1985;26:68–73.

Investigative Ophthalmology & Visual Science